Solving the Couette inverse problem using a wavelet-vaguelette decomposition

Christophe Ancey[a)]

École Polytechnique Fédérale de Lausanne, Ecublens, 1015 Lausanne, Switzerland

(Received 21 June 2004; final revision received 3 November 2004)

Synopsis

This paper develops a new approach to computing the shear rate from the torque and rotational-velocity measurements in a Couette rheometer. It is based on wavelet-vaguelette decomposition (WVD) proposed by Donoho [Donoho, D., Appl. Comput. Harmon. Anal. **2**, 101–126 (1995)]. This decomposition consists in expanding the shear rate into a truncated wavelet series, whose coefficients can be determined by computing the inner products of the wavelet functions with dual functions (vaguelette). Compared to other strategies used for recovering the shear rate such as Tikhonov regularization, the WVD method exhibits greater accuracy and faster convergence. Because of the spatial adaptivity of wavelets, it still performs well when the flow curve is irregular (yield stress, sudden behavior change, etc.) and thus no prior knowledge of the shear rate characteristics (e.g., existence of a yield stress, smoothness) is needed. Its efficiency is demonstrated by applying the method to two fluids (a polymeric gel and a granular suspension). © *2005 The Society of Rheology.* [DOI: 10.1122/1.1849181]

I. INTRODUCTION

A longstanding problem in rheometry is the so-called Couette inverse problem, in which one tries to derive the flow curve $\tau(\dot{\gamma})$ from the torque measurements $M(\omega)$ in a coaxial cylinder (Couette) rheometer, where τ is the shear stress, $\dot{\gamma}$ denotes the shear rate, ω is the rotational velocity of the inner cylinder, and M represents the torque per unit height [Coleman *et al.* (1966)]. The shear stress τ exerted on the inner cylinder of radius R_1 can be directly related to the measured torque M by $\tau=\alpha_1 M$, with $\alpha_1=1/(2\pi R_1^2)$, independently of the form of the constitutive equation. The shear rate is related to the rotational velocity ω by

$$\omega = \int_{R_1}^{R_2} \frac{\dot{\gamma}(r)}{r} dr, \tag{1}$$

where R_2 denotes the outer-cylinder radius and it is assumed that (i) the rotational velocity of the outer cylinder is zero and (ii) there is no slip between the inner cylinder and the sheared material at $r=R_1$. In order to recover the flow curve from measurements of the rotational velocity $\omega(M)$, one must be able to

a)Electronic mail: Christophe.ancey@epfl.ch

(i) relate the function $\dot{\gamma}(r)$ to $\tau(r)$;
(ii) find out a means of inverting the integral relationship (1); and
(iii) estimate the continuous function $\dot{\gamma}(\tau)$ from a set of discrete values (ω_i, M_i).

For a broad class of fluids (simple fluids), the first step is systematically achieved since there is a one-to-one relation between the shear stress and the shear rate for steady viscometric flows: $\dot{\gamma}=\dot{\gamma}(\tau)$. Moreover, the momentum equations imply that the shear stress distribution across the gap is given by $S(r)=M/(2\pi r^2)=\tau(R_1/r)^2$, where r denotes the distance from the vertical rotation axis of the cylinders. Under these conditions, which are not too stringent, it is possible to make the variable change $r=R_1\sqrt{\tau/S}$ in the earlier integral; we then derive the well-known equation [Coleman *et al.* (1966), Krieger and Elrod (1953)]:

$$\omega(\tau)=\frac{1}{2}\int_{\beta\tau}^{\tau}\frac{\dot{\gamma}(S)}{S}dS, \tag{2}$$

where $\beta=(R_1/R_2)^2$. The next step is to recover $\dot{\gamma}$ from $\omega(\tau)$.

Although this problem admits an analytical theoretical solution in the form of an infinite series [Coleman *et al.* (1966)], deriving the shear rate remains a difficult task in practice because the derivation enters the class of ill-posed problems [Friedrich *et al.* (1996)]. In rheometry, the first attempt at solving Eq. (2) can be attributed to Mooney (1931), Krieger and Maron (1952), and Krieger and Elrod (1953). When β is close to unity, it is possible to directly approximate the integral to the first order by

$$\omega(\tau)=\frac{1-\beta}{2}\dot{\gamma}(\tau)+o(\beta\dot{\gamma}).$$

When β moves away from unity, further terms are needed in the expansion of the integral into a β series. Although refined to achieve higher accuracy [Yang and Krieger (1978)], Krieger's approach was unable to provide reliable results for viscoplastic flows [Darby (1985), Nguyen and Boger (1992)] or for data contaminated by noise [Borgia and Spera (1990)]. Alternative methods have been proposed: Tanner and Williams (1970) developed an iterative procedure, whereas Macsporran (1989), Yeow *et al.* (2000), and Leong and Yeow (2003) used a regularized least-square approach, which involves discretizing the integral term and regularizing it.

These methods are very efficient for a wide range of well-behaved rheological equations. However, when the rheological behavior exhibits singularities such as yield stress or a rapid shear thickening, the regularization procedure can lead to unrealistic results by smoothing out the singularities or to complicated trial-and-error loops. For instance, when testing Tikhonov's method with viscoplastic flows, Yeow *et al.* (2000) had to evaluate the yield stress iteratively, which may involve a large number of computations and slow convergence. This undesired behavior is to a large extent the result of attempting to evaluate a continuous function $[\dot{\gamma}(\tau)]$ from a finite set of discrete values representing measurements of bulk quantities. This task is more delicate than believed, especially when data are noisy. For a well-behaved rheological equation, imposing a certain degree of smoothness in the regularization procedures does not entail many problems. On the contrary, for complex rheological responses, it becomes increasingly difficult to discern genuine rheological properties, noise effects, and discretization errors.

The objective of this paper is to propose a new method for recovering the shear rate from the function $\omega(\tau)$, which is numerically stable (no noise amplification) and can deal with irregular functions. The basic idea is to approximate the solution using a finite series

of properly selected functions. We will then show how to invert the integral Eq. (2) using specific properties of this equation. In applied mathematics, a large number of function families are used to approximate functions, e.g., Legendre polynomials, Chebyshev polynomials, trigonometric functions (Fourier expansion), etc., but when the function to be approximated is highly nonlinear or exhibits singularities, the expansion may need an infinite number of terms to be accurate. In that case, it is advantageous to use wavelet functions because these functions have been designed to provide sparse representations of regular and irregular functions [Louis *et al.* (1997)]. Although they are not the cornerstone in the derivation of the method, wavelet functions turn out to be an essential ingredient when applying the method to real data.

The approach developed here takes its roots in a more general mathematical theory referred to as the *adjoint-operator method* proposed by Golberg (1979) and one of its recent extensions called *wavelet-vaguelette decomposition* (WVD). This theory was developed by Donoho (1995) to solve certain classes of inverse problems. Perhaps because of its lack of versatility and the mathematical difficulties arising in its implementation, little research has attempted to apply this technique to solve inverse problems in practical situations {e.g., Kolaczyk (1996) in tomography and [Champier and Grammont (2002)] for particle-size distribution}. In this paper, we will focus on recovering the shear rate from the rotational-velocity measurement in practical cases, whatever the irregularity of the constitutive equation.

Section II will present the different mathematical approaches used so far to solve inverse problems such as the Couette problem. This will help to situate the approach presented here with respect to other techniques. Two formulations of the WVD method will be outlined:

- a continuous formulation (Sec. III), in which the rotational velocity is a given continuous function. In practice, this means that the measurements (ω_i, M_i) are interpolated to provide a smooth function assumed to give a correct representation of the function $\omega(\tau)$. In this way, we separate problems (ii) and (iii) earlier; and
- a discrete formulation (Sec. A in the Appendix), where the only information we have are measurements of the rotational velocity. In the same process, we are trying to invert Eq. (2) [problem (ii)] and infer the local relationship $\dot{\gamma}(\tau)$ from a finite set of measurements taken on the macroscopic scale (ω_i, M_i) [problem (iii)].

In Sec. IV, we apply the WVD method to two fluids (a viscoplastic polymeric gel and a granular suspension exhibiting an unusual rheological behavior), and we show its efficiency in recovering the flow curve compared to the regularized least-square method (Tikhonov's method). The mathematical proofs and a Mathematica package for rheometric applications are available as an EPAPS document; see the Reference section for the details.

II. MATHEMATICAL STRATEGY

In the Couette inverse problem, Eq. (2) can be represented in the generic form: $\omega(\tau) = (K\dot{\gamma})(\tau)$, where K is the integral operator

$$(Kf)(z) = \int_{\beta z}^{z} \frac{f(x)}{x} dx, \tag{3}$$

with β a constant parameter ($\beta < 1$). A considerable body of literature has been published over the last three-decades on ill-posed inverse problems in this form [Bertero *et al.*,

(1985, 1988), O'Sullivan (1986), Tenorio (2001)]. Schematically, we can split the various methods for solving Couette-like problems into three main categories.

- *Least-square approach*: instead of solving $\omega = K\dot{\gamma}$, an attempt is made to minimize the residual $\|\omega - K\dot{\gamma}\|$, usually with an additional constraint on the norm of $\|f\|$ or its derivative(s), to control the smoothness of the solution. Tikhonov's regularization method used by Yeow *et al.* (2000) and Landweber's iterative procedure used by Tanner and Williams (1970) come within this category. The advantages of this method are its robustness against computation inaccuracies and measurement errors, its versatility, its fast convergence when the function to be recovered behaves reasonably well, and the relative facility of its implementation. The drawbacks are that it relies on an arbitrary selection of the regularization operator (even though specific procedures have been established) and its limited capacity to retrieve irregular functions.
- *Projection approach*: the idea here is to discretize the problem by projecting the function over a finite space spanned by a family of functions enjoying specific properties (such as orthogonality) u_i. Equation (2) is then replaced by the finite set of equations $\langle K\dot{\gamma}, u_i \rangle = \langle \omega, u_i \rangle$ for $1 \leqslant i \leqslant p$, where $\langle f, g \rangle = \int_{\mathbb{R}} f(x)g(x)dx$ denotes the inner product in the function space [Dicken and Maass (1996), Louis *et al.* (1997), Rieder (1997)]. Galerkin's method, used by Macsporran (1989) with spline functions, provides a typical example for Couette rheometry. Irregular functions can be recovered by these methods provided appropriate projection functions are chosen in advance.
- *Adjoint operator approach*: for many reasons, it is usually either not possible or not advantageous to compute the inverse operator K^{-1}. In some cases, however, it is possible to provide a weak inverse formulation, in which the function $\dot{\gamma}$ is expressed as

$$\dot{\gamma} = \sum_{i \in J} \langle K\dot{\gamma}, u_i \rangle \Psi_i,$$

  where the summation is made over a set J, Ψ_i is an orthonormal basis of functions, and u_i denotes a family of function solutions of the adjoint problem $K^* u_i = \Psi_i$, where K^* is the adjoint operator of K [Golberg (1979)]. Typical examples include *singular-value decomposition* [Bertero *et al.* (1985, 1988)], a generalized formulation based on *reconstruction kernels* [Louis (1999)], *wavelet-vaguelette decomposition* [Donoho (1995)], and *vaguelette-wavelet decomposition* [Abramovich and Silverman (1998)]. The solution to the inverse problem is found by replacing $K\dot{\gamma}$ with ω in the equation earlier and filtering or smoothing the inner products $\langle K\dot{\gamma}, u_i \rangle$ and/or truncating the sum.

This partitioning is a bit arbitrary because there are interconnections between the three categories {e.g., Tikhonov's regularization can be viewed as a special case of singular-value decomposition [Bertero *et al.*, (1988)]}. This is, however, sufficient in the present paper to outline the main approaches used so far and to situate the previous attempts at solving the Couette problem. Alternative methods, e.g., stochastic methods [Gamboa and Gassiat (1997); Mosegaard and Sambridge (2002)], are also possible, but have never been used in rheometry as far as we know.

Here we will develop a strategy based on wavelet-vaguelette decomposition. The wavelet functions are orthonormal functions generated from dilations and translations of a special function, called the *mother wavelet* ψ (see the EPAPS document for an introduction to their useful properties or any textbook on wavelets) and associated with another function called the *father wavelet* or the *scaling function* ϕ. One of their most interesting properties is that, for some classes of mother wavelet such as Daubechies wavelets, it is possible to know the convergence rate and the accuracy of the solution in

advance. A large part of their success lies in their spatial adaptivity: contrary to other families of orthogonal functions (Legendre, Chebyshev, trigonometric, etc.), wavelets are well localized and scale-dependent, which makes it possible to provide sparse representations of regular and irregular functions.

III. FUNCTIONAL FORMULATION OF WAVELET-VAGUELETTE DECOMPOSITION

A. Principle

We will begin by exposing the principle in a very simple manner. A more rigorous mathematical derivation follows. Let us assume that we can approximate any shear rate function $\dot{\gamma}(\tau)$ with a finite series of terms

$$\dot{\gamma}(\tau) \approx \sum_k a_k \Psi_k(\tau),$$

where Ψ_k denotes the kth member of a family of orthogonal functions, i.e., $\int \Psi_k(\tau)\Psi_i(\tau)d\tau = \delta_{ik}$; making use of this property, we could compute the coefficients a_k as $a_k = \int \dot{\gamma}(\tau)\Psi_i(\tau)d\tau$ if the function $\dot{\gamma}(\tau)$ were known.

Using the linearity of the integral operator K, we have

$$\omega(\tau) = (K\dot{\gamma})(\tau) \approx \sum_k a_k (K\Psi_k)(\tau).$$

Note that the function $\omega(\tau)$ shares the same coefficients a_k as the shear-rate function, implying that if we were able to expand $\omega(\tau)$ into a $(K\Psi_k)$ series, we could determine the coefficients a_k, then find an approximation of $\dot{\gamma}(\tau)$.

Unfortunately, the functions $(K\Psi_k)(\tau)$ are not orthogonal, making it difficult to numerically compute a_k. Specific procedures such as the Schmidt orthogonalization procedure could be used to derive an orthogonal family of functions from $(K\Psi_k)(\tau)$, but here this involves overly complicated computations. We will envisage another technique based on dual bases. A dual basis of the function basis $(K\Psi_k)$ is a set of functions u_i such that $\int u_i(\tau)(K\Psi_k)(\tau)d\tau = \delta_{ik}$, implying that $a_k = \int \omega(\tau)u_k(\tau)d\tau$. Therefore the crux of the issue lies in the derivation of the dual basis u_k. In the following, we will show that the functions u_k can be built from the functions Ψ_i.

B. Mathematical derivation

In mathematically formulating the problem, we wish to find an approximate solution of the problem: $(Kf)(x) = g(x)$, where $g(x)$ is a given function. The approximate solution is defined as the approximation of the true solution f by expanding it into a finite series of functions Ψ_k:

$$\tilde{f} = \sum_{k=0}^{p-1} a_k \Psi_k,$$

where Ψ_k is a set of orthonormal independent functions, with a finite support (Ψ_k takes nonzero values on a finite interval) and indexed by k, p is the number of functions needed to approximate f, and $a_k = \langle f, \Psi_k \rangle$. The brackets $\langle f, \Psi_k \rangle$ are a shorthand notation standing for the scalar product of the functions f and Ψ_k, defined as follows: $\langle f, \Psi_k \rangle = \int_D f(x)\Psi_k(x)dx$, the integration being made on an interval D (e.g., $\mathbb{R}$ or the interval over which Ψ_k is defined).

We denote the image of Ψ_k by $v_k(x)=K\Psi_k(x)$. We also introduce the adjoint of the operator K, denoted by K^*. The adjoint operator is defined in such a way that: $\langle Ka,b\rangle = \langle a,K^*b\rangle$ for any function a or b. After basic integral computations (integration by parts), it can be shown that the adjoint operator is

$$(K^*g)(x) = \frac{1}{2x}\int_{x/\beta}^{x} g(y)dy. \tag{4}$$

If we can find a dual function u_k such that $\Psi_k = K^*u_k$, then we obtain the biorthogonality relationship

$$\langle u_i, v_j\rangle = \delta_{ij}.$$

Indeed we have $\langle u_i,v_j\rangle = \langle K\Psi_i,v_j\rangle = \langle \Psi_i,K^*v_j\rangle = \langle \Psi_i,\Psi_j\rangle = \delta_{ij}$. We are trying to solve the approximate inverse problem

$$K\tilde{f} = \sum_{k=0}^{p-1} a_k v_k = g.$$

Multiplying by function u_k and integrating over $\mathbb{R}$, we obtain the reproducing formula

$$\tilde{f} = \sum_{k=0}^{p-1} \langle K\tilde{f},u_k\rangle \Psi_k = \sum_{k=0}^{p-1} \langle g,u_k\rangle \Psi_k. \tag{5}$$

Consequently the key step in the treatment is to find the dual function basis $(u_k)_{0\leqslant k\leqslant p-1}$. It can be shown that the dual basis can be obtained by posing

$$u_k(x) = -\sum_{i=0}^{\infty} \frac{1}{\beta^i} U_k'\left(\frac{x}{\beta^i}\right), \tag{6}$$

where $U_k(x)=x\Psi_k(x)$. Indeed, for $i=0$, using an integration by parts, we obtain

$$\langle K\Psi_j(x),-U_k'(x)\rangle = -\left[K\Psi_j(x)U_k(x)\right]_{-\infty}^{+\infty} + \int_{-\infty}^{+\infty}\left(\frac{\Psi_j(x)}{x} - \frac{\Psi_j(\beta x)}{x}\right)x\Psi_k(x)dx.$$

Since Ψ_k has a finite support [implying $K\Psi_j(x)=0$ when $x\to\pm\infty$], we obtain

$$\langle K\psi_j(x),-U_k'(x)\rangle = \delta_{jk} - \int_{-\infty}^{+\infty}\psi_j(\beta x)\Psi_k(x)dx = \delta_{jk} - \frac{1}{\beta}\int_{-\infty}^{+\infty}\Psi_j(x)\Psi_k(x/\beta)dx.$$

Repeating the procedure for $i>0$, we can show that $\langle K\psi_j(x),u_k(x)\rangle = \delta_{jk}$. When taking the inner product with any function g such that $g=Kf$, the convergence is ensured here because $\beta<1, g(0)=0$, and $g'(0)$ is finite; indeed, we have

$$\beta^{-i}\langle g(x),U_k'(\beta^{-i}x)\rangle = \langle g(x\beta^i),U_k'(x)\rangle \approx \beta^i\langle g'(0),U_k'(x)\rangle + O(\beta^i),$$

when i is sufficiently large. Asymptotically, we find that $\beta^{-i}\langle g(x),U_k'(\beta^{-i}x)\rangle$ behaves like β^i, implying that $\langle K\psi_j(x),u_k(x)\rangle$ converges to a well-defined limit.

When coping with irregular functions or when interested in obtaining sparse representations of functions, it is advantageous to use wavelet functions for the orthonormal basis Ψ_k. Another advantage in using wavelets is that the convergence rate and an estimate of the error made in expanding the solution into a wavelet series can be determined in advance (see the EPAPS document). When wavelet functions are used, the dual basis functions u_i are called *vaguelettes* by Donoho (1995) because they present properties that

are very close to properties exhibited by wavelets. In the following, we will use the so-called Daubechies D8 wavelets for Ψ_k, but alternative choices can also be made without significant changes in the final result.

C. Numerical implementation

The numerical implementation of the method is reasonably simple since it involves computing the inner products $\langle \omega(\tau), u_k(\tau) \rangle$. Several commercial products (Mathematica, Mathlab, etc.) allow such computations. For numerical purposes, it is convenient to use dimensionless variables. We can take dimensionless variables by defining $\omega = \Omega \omega_{\max}$, $\dot{\gamma} = \Gamma \omega_{\max}$, and $\tau = T \tau_{\max}$, where $\tau_{\max}$ and $\omega_{\max}$ denote, respectively, the maximum shear stress and rotational velocity. The dimensionless operator has the same form as the original

$$\Omega(T) = (K\Gamma)(T) = \int_{\beta T}^{T} \frac{\Gamma(\xi)}{\xi} d\xi, \tag{7}$$

but it is defined for functions taking their values on $[0, 1]$ instead of $\mathbb{R}$. A Mathematica program doing the numerical calculations is included in the EPAPS document. This program includes both WVD decomposition and Tikhonov's method.

In practical situations, function $\Omega(T)$ must be evaluated from data, e.g., by using interpolation techniques such as the kernel method or wavelet regression [Hart (1999); Kovac (1998); Wahba (1990)]; the inner products can then be computed by numerical integration of this interpolating curve.

Computation time and convergence can be accelerated; instead of solving the problem Eq. (7), we can solve the problem

$$\Omega(T) = (K\Gamma)(T) = \int_{\beta T}^{T} \Lambda(\xi) d\xi, \tag{8}$$

where $\Lambda(\xi) = \Gamma(\xi)/\xi$. In this case, the dual vector is $u_i = -\Sigma_{k=0}^{\infty} \beta^{-k} \Psi_i'(\beta^{-k} x)$; thus, in determining the inner product $\langle \Omega(T), u_k(T) \rangle$, the trick is to compute $\langle \Omega(T), \Psi_i'(T) \rangle$, whereas in the original problem, $\langle \Omega(T), x\Psi_i'(T) + \Psi_i(T) \rangle$ must be computed.

The inner product involves the dual vectors u_i, defined from an infinite series [see Eq. (6)]. In practice, the series is truncated when β^i is small enough. Typically, for $\beta = 0.5$, keeping the first ten terms of the series is sufficient to ensure an accuracy of 10^{-3}.

When the material is viscoplastic, the shear rate is nonzero only for a shear stress in excess of the yield stress τ_c. As a consequence, some authors replace the lower bound $\beta\tau$ in Eq. (2) with τ_c [Nguyen and Boger (1992); Yeow *et al.* (2000)]. In the numerical computations, this replacement may increase accuracy and avoid problems of vanishing shear rates, but this also implies that one of the integration bounds is not known and must be determined separately or iteratively [e.g., see Yeow *et al.* (2000)]. A clear advantage of the method presented here is that the wavelet functions are specifically designed to capture possible discontinuities and consequently it is not necessary to modify the integration bounds. Note that, when using the Tikhonov regularization technique, it is possible to keep the integral boundaries unchanged by writing

$$\omega(\tau) = \frac{1}{2} \int_{\tau_c}^{\tau} \frac{\dot{\gamma}(S)}{S} dS = \frac{1}{2} \int_{\beta\tau}^{\tau} \frac{\dot{\gamma}(S)}{S} H(S - \tau_c) dS,$$

where H denotes the heavyside function.

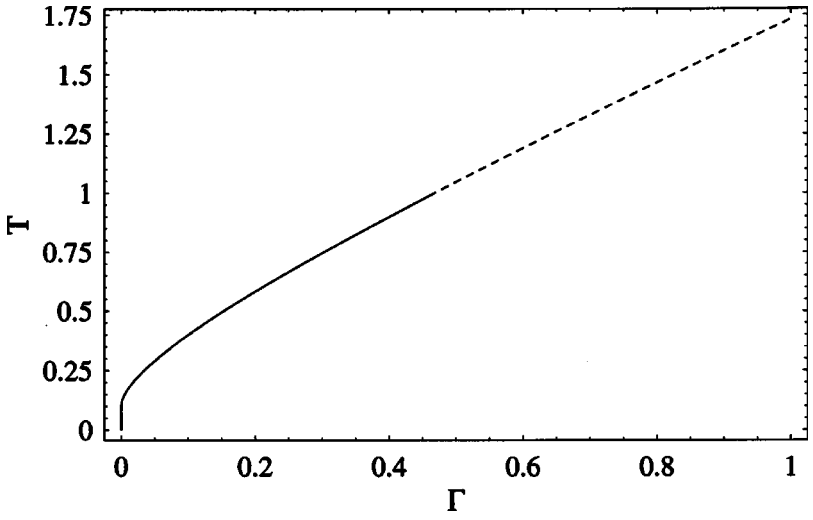

FIG. 1. Flow curve for the (dimensionless) Casson model. The solid line represents the numerical approximation obtained by using the WVD approach, whereas the dashed line represents the exact solution Eq. (9).

D. Numerical example

For the numerical test, let us consider the following Casson constitutive equation in a dimensionless form

$$\sqrt{T} = \sqrt{T_c} + \sqrt{\Gamma}, \tag{9}$$

where T_c is the dimensionless yield stress. For numerical applications, let us set $T_c = 0.1$. Computations are made over the interval [0, 1]. The corresponding dimensionless torque per unit height is

$$\Omega(T) = \begin{cases} 0 & \text{for } T < T_c, \\ T - T_c - \sqrt{TT_c} + 4T_c + T_c \ln(T/T_c) & \text{for } T_c \leqslant T < \beta T_c, \\ T_c - \beta T + 4\sqrt{TT_c}(\sqrt{\beta} - 1) - T_c \ln\beta & \text{for } T \geqslant \beta T_c. \end{cases} \tag{10}$$

We use the Daubechies D8 father wavelets ϕ. To represent functions whose support lies within [0, 1], $p = 78$ wavelets are needed; we use $(\Psi_k)_{1 \leqslant k \leqslant 78} = \{\phi_{6,-14}, \phi_{6,-13}, \cdots, \phi_{6,63}\}$. We denote $\widetilde{\Gamma}$ the approximate dimensionless shear rate. The recovered shear rate is reported in Fig. 1. Note the perfect reconstruction of the shear rate over the entire interval. The mean-square error is approximately $1.219\,65 \times 10^{-9}$ vs $1.216\,75 \times 10^{-9}$ when $\widetilde{\Gamma}$ is computed from the exact function.

Similar tests were carried out by replacing the exact dimensionless torque with an interpolating polynomial (piecewise polynomial of order 3) fitting $n_d = 100$ data computed from $\Omega(i\delta)$, for $i = 0, \ldots, n_d - 1$ and $\delta = (n_d - 1)^{-1}$. Very good agreement was found, with no difference to the naked eye with the exact flow curve (mean-square error $1.296\,932 \times 10^{-9}$).

In parallel, we used the Tikhonov method as described in [Yeow *et al.* (2000)]; we used the same set of n_d simulated data $\Omega(i\Delta)$, $n_k = 200$ interpolation points to discretize the integral term in Eq. (7) and a smoothing parameter $\lambda = 10^{-6}$. The result is reported in Fig. 2(a). Good agreement was also found for this method between the exact flow curve and the recovered curve, but the mean-square error is substantially larger than for the

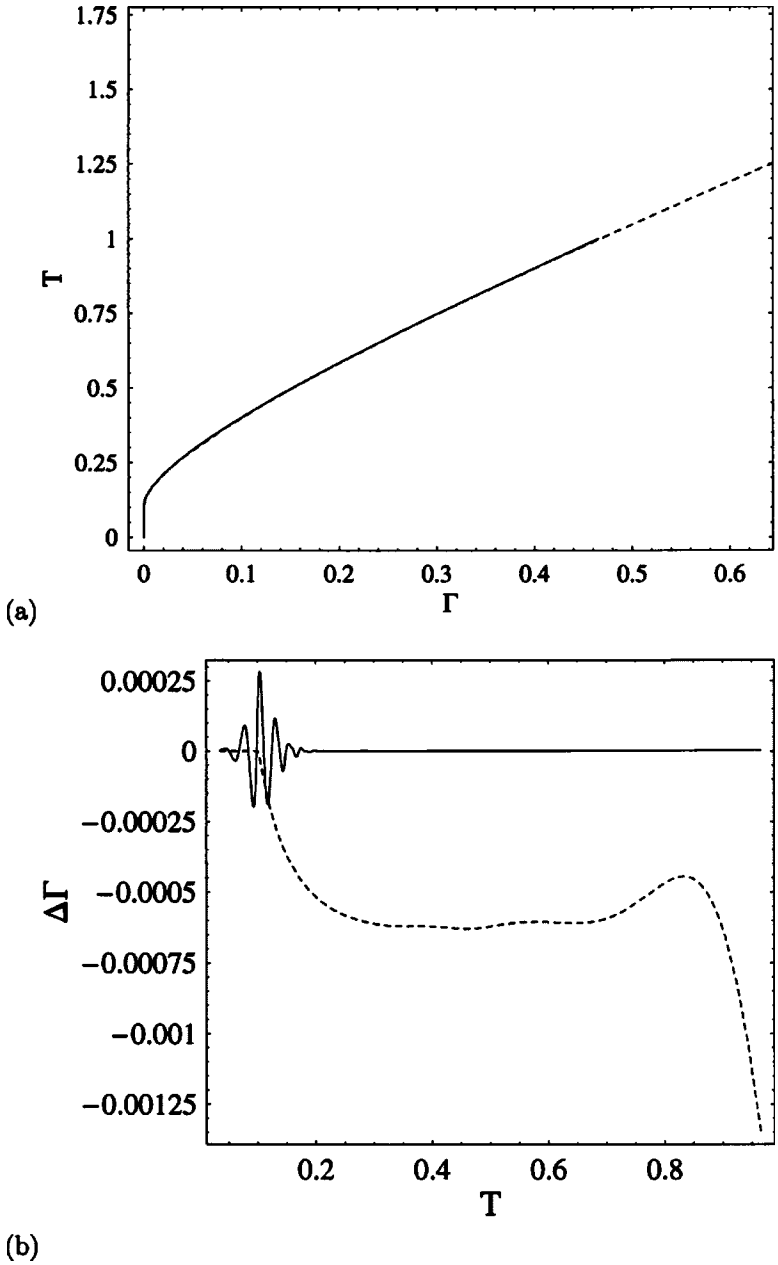

FIG. 2. (a) Flow curve for the (dimensionless) Casson model when Tikhonov's method is used; the solid line represents the numerical approximation obtained by using the Tikhonov approach, whereas the dashed line represents the exact solution [Eq. (9)]. (b) Difference between the computed and the exact shear rates (bias) as a function of the dimensionless shear stress: WVD approach (solid line) vs Tikhonov method (dashed line).

WVD approach (2.52×10^{-6} vs 1.29×10^{-9}). The main difference between the two methods lies essentially in the bias between the exact flow curve and the reconstructed curve. As shown in Fig. 2(b), the difference $\Delta\Gamma$ between the recovered value and the exact shear rate is very close to zero for the WVD method apart from the yielding point at $T=0.1$, whereas it is systematically below zero for the Tikhonov method and increases with increasing stress T.

IV. APPLICATION TO REAL CASES

A. Raw data

We have applied both the WVD inverse method and Tikhonov's regularization technique to two series of data available in the literature.

- Baudez *et al.* (2004) investigated the rheological properties of a polymeric suspension (commercial hair gel made of Carbopol) using a stress-controlled Paar Physica MC1 + rheometer equipped with a Couette geometry ($R_1 = 1.25$ cm and $\beta = 0.26$). In addition they carried out velocity-profile measurements in a similar geometry ($R_1 = 4$ cm and $\beta = 0.44$) using magnetic resonance imaging (MRI) techniques. Further rheometrical tests were also done with a Bohlin CVOR200 rheometer ($R_1 = 0.0125$ cm and $\beta = 0.06$). Carbopol suspensions usually exhibit a viscoplastic behavior [Roberts and Barnes (2001)]. MRI techniques made it possible to obtain an accurate estimation of the flow curve and then to compare the different methods.
- Ancey (2001) studied the rheological behavior of granular suspensions using a vane mounted on a Haake Rotovisco MV5 rheometer ($R_1 = 3$ cm and $\beta = 0.09$); the sheared height was $h = 32$ mm (different heights were also tested). The tested suspension was made up of glass beads (diameter 0.8 mm) in a 98.5% water/glycerol solution at the solid concentration of 60% (very close to the maximal solid concentration). Such suspensions exhibit a complicated behavior depending on the shear rate: a frictional Coulombic behavior at low shear rates (like a granular soil) and viscous behavior at high shear rates.

The data obtained by Baudez *et al.* (2004) and Ancey (2001) are reported in a log-linear plot in Fig. 3. They were slightly noisy and a specific procedure was used to denoise and interpolate the raw data. Different nonparametric regression techniques can be used for this purpose: kernel estimator [Hart (1999)], spline smoothing [Wahba (1990)], Fourier series estimator, wavelet regression and shrinkage [Cai (1999, 2002); Donoho and Johnstone (1995); Kovac (1998)], Bayesian inference [Werman and Keren (2001)], etc. There is not a universal method because, depending on the noise level, the number of data, and the properties of the function to be recovered, the performance of each method in terms of denoising efficiency can vary significantly. Here, because of the small size of the data samples, the optimized Gasser–Müller kernel method (included in the Mathematica package) was used to denoise and interpolate the data {for details in the implementation, see [Hart (1999)]}. The resulting interpolating curves are plotted in Fig. 3.

B. Results

Figure 4 shows the flow curves deduced by the Tikhonov regularization method (dashed line) and the wavelet-vaguelette decomposition method (solid line) for the polymeric gel and the granular suspension. For the Tikhonov method, we used the method described in [Yeow *et al.* (2000)] with $n_k = 400$ discretization points and a smoothing parameter $\lambda = 2 \times 10^{-6}$ and 5×10^{-6} for the polymeric gel and the granular suspension, respectively. For the WVD method, Daubechies D8 wavelet and the functional formulation were used (see Sec. III).

For the polymeric gel, it was possible to independently obtain a reference flow curve by using the velocity profile determined by Baudez *et al.* (2004) using MRI techniques. Indeed, in a Couette geometry, the shear stress distribution across the gap is imposed: $\tau(r) = M/(2\pi r^2)$; the shear rate can be computed by differentiating the velocity profile

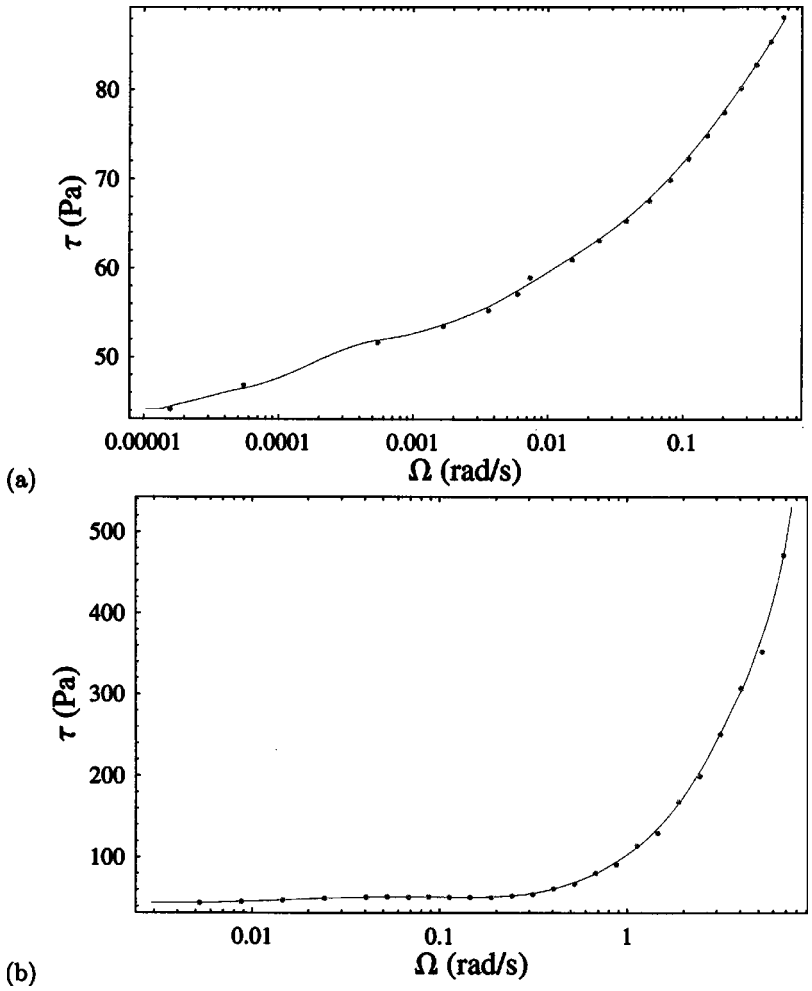

FIG. 3. (a) Raw data obtained by Baudez *et al.* (2004) for a polymeric gel (Carbopol). (b) Raw data obtained by Ancey (2001) for a granular suspension. Dots correspond to data while the solid lines represent the curve interpolating the data obtained using the Gasser–Müller kernel method [bandwidth parameter taken at 0.1 (a) and 0.05 (b)].

$v(r)$: $\dot{\gamma}(r) = -r\,\partial(v/r)/\partial r$. Reporting a parametric plot $[\dot{\gamma}(r), \tau(r)]$ as a function of the radial distance r makes it possible to have a clearer idea on the flow curve for the material tested. The dots in Fig. 4(a) represent the flow curve determined in this way.

For the polymeric gel [see Fig. 4(a)], the three methods compare well over a shear-rate range covering approximately two orders of magnitude ($5 \times 10^{-2} \leqslant \dot{\gamma} \leqslant 20\ \mathrm{s}^{-1}$), whereas differences can be observed at low and high shear rates. Because of the smoothing constraint imposed on the flow curve in the Tikhonov method, the shear stress drops quickly at low shear rates, leading to an underestimation of the yield stress (estimated at 41 Pa using independent tests). Similarly, at large shear rates, the slight convexity of the flow curve (in a log-linear representation) leads to an undue increase in the shear stress. Because of the absence of regularization constraint in the WVD method, the corresponding flow curve comes closer to the experimental flow curve inferred from MRI measurements. We can, however, notice the bump for shear rates in the range 10^{-3}–5

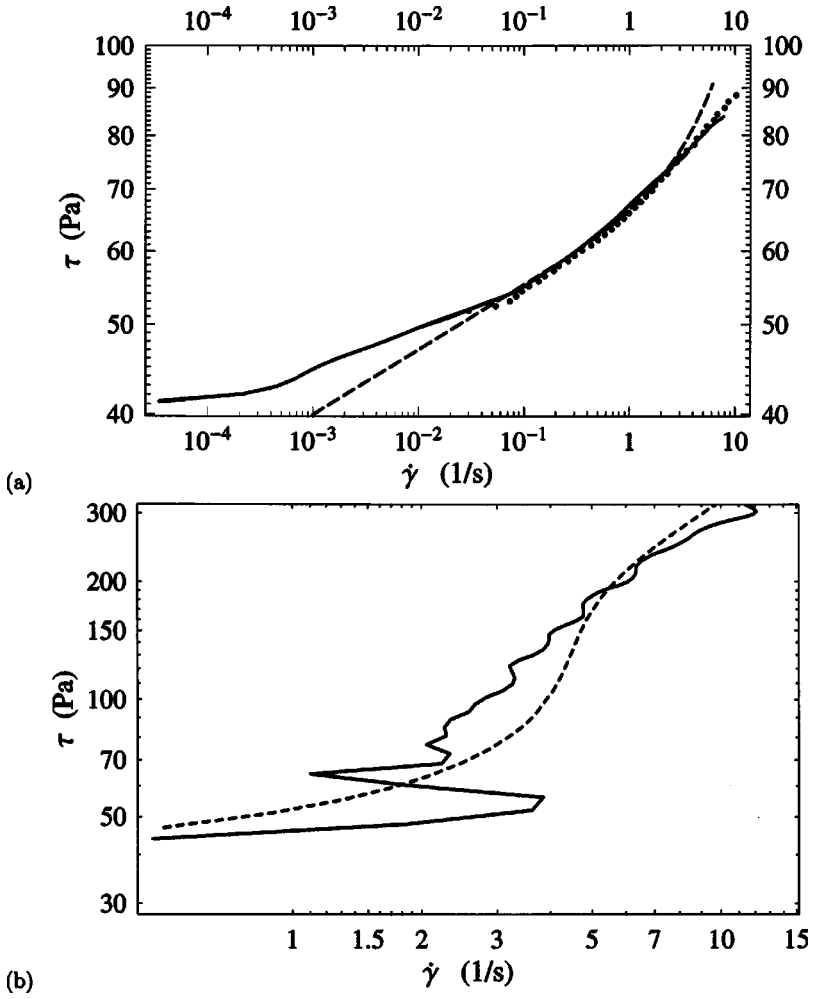

FIG. 4. (a) Flow curve for the polymeric gel. (b) Flow curve for the granular suspension. In (a), the dots represent the flow curve obtained by differentiating the MRI velocity profile. The dashed lines represent the flow curves obtained using the Tikhonov method [smoothing parameter $\lambda = 2 \times 10^{-6}$ and $\lambda = 5 \times 10^{-6}$ for flow curves (a) and (b), respectively]. The solid lines represent the flow curve determined using the WVD method.

$\times 10^{-2}$ s^{-1}, which seems not natural. This is probably an artifact caused by the interpolating curve [see Fig. 3(a)] since a similar bump is also observable. Additional rotational-velocity data are required to improve accuracy in the low-shear-rate limit.

For the granular suspension, substantial differences appear between the flow curves deduced using the Tikhonov and WVD methods. At first glance, the WVD flow curve shows an unrealistic wiggly behavior while the Tikhonov flow curve seems more realistic and to smooth out the shear-stress oscillations seen in the WVD curve. The behavior exhibited by the WVD solution can be understood by reminding the main traits of the bulk behavior [Ancey (2001)].

- At low shear rates, the granular suspension exhibited a frictional Coulombic behavior, i.e., a shear-rate independent shear stress, which was linearly linked to the normal

stress; shear was localized within a narrow cylindrical band around the vane, whose typical size was a few diameters.
- At large shear stress, the suspension behavior was closer to a Newtonian behavior ($M \propto \Omega$ and τ independent of the normal stress); all the space between the vane and outer cylinder was sheared.

This regime transition was interpreted as a consequence of contact lubrication between particles [Ancey (2001)]. As seen in Fig. 3(b), the transition between the two regimes occurred at approximately $\Omega = 0.4$ rad/s. Since the typical thickness was of the order of 5–10 particle diameters, i.e., 4–8 mm, we deduce that the critical shear rate at the transition was of the order of $\dot{\gamma}_c = 0.03 \times 0.4/(4 \times 10^{-3}) = O(2)\text{s}^{-1}$. When contacts between particles were lubricated, the shear-band thickness rapidly grew to finally occupy all the available space, leading to a progressive decrease in the shear rate. If the expansion of the sheared region were instantaneous at the transition, the shear rate should have dropped to a minimum value, whose order of magnitude is $\dot{\gamma}_m = 0.03 \times 0.4/0.1 = O(0.1)\text{s}^{-1}$.

Taking a closer look at the WVD solution [see Fig. 4(b)], we observe that, for low shear stresses ($\tau < 50$ Pa), the flow curve is approximately horizontal for shear rates in the range $0.1-4\ \text{s}^{-1}$. At $\dot{\gamma} = 4\ \text{s}^{-1}$ (close to the order of magnitude found for $\dot{\gamma}_c$), a slight increase in the shear stress leads to a substantial decrease in the shear rate, which drops to $1\ \text{s}^{-1}$; this value is much higher than the value of $\dot{\gamma}_m$, but this is normal since $\dot{\gamma}_m$ has been estimated by assuming a sudden expansion of the sheared zone. For higher shear stress ($\tau > 80$ Pa), the shear stress varies almost linearly with increasing shear rates.

Variants of the WVD decomposition and interpolation techniques were used, but we came to similar conclusions. In brief, although, at first sight, it was a bit unrealistic, the behavior exhibited by the WVD solution can be convincingly explained by analyzing the bulk behavior {reflected in the scaling behavior of $M(\Omega, h)$ shown in [Ancey (2001)]} and interpreting it in terms of particle behavior. For the same reason as for the polymeric gel, the Tikhonov solution smooths the flow curve bulges, thus it compares well with the WVD solution only at very low and large shear rates ($\dot{\gamma} < 1\ \text{s}^{-1}$ or $> 6\ \text{s}^{-1}$).

V. DISCUSSION AND CONCLUDING REMARKS

In this paper we have shown that the wavelet-vaguelette decomposition makes it possible to recover the shear rate $\dot{\gamma}$ from the rotational velocity $\omega(\tau)$ by using a wavelet representation

$$\dot{\gamma}(\tau) = \sum_k g_k \Psi_k(\tau),$$

where Ψ_k is a wavelet basis and $g_k = \langle \omega(\tau), u_k \rangle$ with the vaguelette function $u_k(\tau) = -\Sigma_k \beta^{-k} [\tau \Psi_k(\tau)]'(\beta^{-k}\tau)$. Wavelet bases offer accurate and sparse representations for functions whatever their regularity. Therefore, for most cases encountered in rheometry, it is possible to reconstruct the shear rate $\dot{\gamma}$ from the rotational velocity ω without using additional assumptions on the smoothness of $\dot{\gamma}$, as in Tikhonov's regularization. Another advantage offered by the WVD approach is that, fundamentally, very high accuracy can be imposed in advance when reconstructing the shear rate by an appropriate selection of the wavelet basis and the number of elements used in the wavelet representation. Traditional methods such as Galerkin methods or the regularized least-square approach do not lead to such a high degree of accuracy and adaptivity unless specific iterative procedures are used to improve the initial results.

When the rotational velocity is a noisy signal, it is possible to remove a large part of the noise by shrinking the wavelet coefficients or smoothing the data.

- Donoho (1995) and Cai (2002) showed that if the shrinkage threshold is properly chosen, then the WVD solution converges toward the "better" solution at the optimal rate. This optimal rate is, however, quite low and thus in practice, a large number of data (typically as large as 2^9) are needed to offset this slow convergence.
- In practice, when the data number is small, alternative regression techniques such as the spline interpolation or the kernel estimator must be used. Here, the optimized Gasser–Müller kernel {see [Hart (1999)]} method was successful in denoising and interpolating experimental data.

In other methods such as the regularized least-square method, noise is smoothed out when regularizing the solution. In a sense, this procedure is more robust and less data hungry because additional assumptions on the smoothness of $\dot{\gamma}$ are used, but it introduces a bias between the exact solution and the regularized curve, which can lead to significant estimation errors in some pathological cases. An exemple has been provided in Sec. IV with a highly concentrated granular suspension.

We have developed two formulations of the wavelet-vaguelette decomposition: continuous and discrete formulations.

- In the continuous case, $\omega(\tau)$ must be a function, evaluated by interpolating data and satisfying $\omega(0)=0$ and $\omega'(0)=c$, where c is a constant for the inner products to converge. Numerical computation of the inner products $g_k=\langle \omega(\tau), u_k \rangle$ can be time consuming, especially when β is close to unity, because the vaguelette functions comprise an infinite series of terms. In principle, any degree of accuracy can be achieved by the WVD decomposition by altering the number p of wavelets and vaguelettes used in the computations (see the EPAPS document), but in practice, there are some restrictions in the maximum achievable accuracy because interpolating functions are used.
- In the discrete case, $\mathbf{w}=\omega(\tau_i)$ is a data vector. To some extent, the discrete formulation can be seen as the discretized version of the continuous WVD decomposition, since the discrete vaguelette is a vector whose points can be interpolated by the corresponding continuous vaguelette (see the Appendix).

In summary, the new method developed here is an interesting alternative to traditional methods such as the Galerkin and Tikhonov methods because it offers greater accuracy. This point is of great importance because a number of materials currently investigated, notably in the field of suspensions, exhibit particular properties, including rapid change behavior in the flow curve {e.g., in glass-bead/glycerol suspensions [Ancey (2001)], clay-water dispersions [Coussot (1995)], etc.}, discontinuous shear rate distribution at the yielding point [Raynaud *et al.* (2002)], giant fluctuations [Lootens *et al.* (2003)], etc. For such materials, the additional assumptions used in the traditional methods (such as the regularization procedure in the Tikhonov method) may lead to unrealistic results. Typical exemples have been provided in Sec. IV.

The wavelet-vaguelette approach is also interesting because (i) it allows us to control the solution accuracy and convergence and (ii) it can be combined with an optimal denoising procedure when data are noisy. Its main drawback lies in the numerical implementation (numerical integration needed until faster algorithms are available) and the computation time that can be much longer than for traditional methods. This approach probably clears the way for other methods that will combine the accuracy and adaptivity of wavelets and the versatility and easiness of Galerkin methods.

ACKNOWLEDGMENTS

This study was supported by the École Polytechnique Fédérale de Lausanne and the Swiss National Science Foundation (Grant No. 200021-105193/1). The author is grateful to Philippe Coussot for providing him with the raw data of the polymeric gel used in [Baudez *et al.* (2004)].

APPENDIX : DISCRETE FORMULATION WAVELET-VAGUELETTE DECOMPOSITION

A. Principle

Here we consider an alternative formulation of the wavelet-vaguelette decomposition, where the discrete nature of experimental data is directly taken into account. We assume that we have n data $\omega_i=\omega(\tau_i)$. The objective is to deduce the shear rate from the rotational-velocity measurements.

To that end, we introduce the discrete operator K_n that maps $L_2(\mathbb{R})$ to $\mathbb{R}^n$, where L_2 represents the space of functions that are square integrable, and its adjoint operator K_n^*:

$$K_n{:}f(x) \rightarrow \mathbf{y}{:}y_i = (Kf)(x_i) = \int_{\beta x_i}^{x_i} \frac{f(z)}{z} dz, \quad 1 \leqslant i \leqslant n,$$

$$K_n^*{:}\mathbf{y} = (y_i)_{1\leqslant i\leqslant n} \rightarrow h(z) = \sum_{i=1}^{n} \frac{y_i}{z} H[(x_i - z)(z - \beta x_i)],$$

where H denotes the heavyside function. The shear rate is related to measurements by $\omega_i=(K_n\dot{\gamma})(\tau_i)$.

As previously, we consider the approximate solution to the inverse problem $K_nf=\mathbf{y}$ by using a truncated wavelet series for the function to be determined: $\tilde{f}=\Sigma_{i=0}^{p-1}a_k\Psi_k$, where Ψ_k is a set of pairwise orthogonal, independent functions. The image of a basis function Ψ_k is denoted by $\mathbf{e}_k=K_n\Psi_k$, i.e., a vector in $\mathbb{R}^n$ (the same holds for the dual basis). We are seeking a dual basis or vaguelette $\tilde{\mathbf{e}}_j$ such that $[\tilde{\mathbf{e}}_j,\mathbf{e}_k]=0$, where the square brackets denote the scalar product in $\mathbb{R}^n$. From the relation

$$[\mathbf{e}_i,\tilde{\mathbf{e}}_k] = [K_n\Psi_i,\tilde{\mathbf{e}}_k] = \langle \Psi_i, K_n^*\tilde{\mathbf{e}}_k\rangle = \delta_{ik},$$

we deduce that Ψ_i and $K_n^*\tilde{\mathbf{e}}_k$ are parallel. In other words, a factor ζ_i exists such that $\zeta_i\Psi_i=K_n^*\tilde{\mathbf{e}}_i$. It follows that:

$$a_i = \langle f,\Psi_i\rangle = \langle f,\zeta_i^{-1}K_n^*\tilde{\mathbf{e}}_{ij}\rangle = \zeta_i^{-1}[K_nf,\tilde{\mathbf{e}}_i].$$

An estimate of the wavelet coefficient a_i is obtained by replacing K_nf by $\mathbf{y}{:}\,a_i=\langle f,\Psi_i\rangle \approx \zeta_i^{-1}[\mathbf{y},\tilde{\mathbf{e}}_i]$.

Different methods can be used to determine the dual basis $\tilde{\mathbf{e}}_i$. Let us call $\mathbf{P}$ the $n\times p$ matrix, whose kth column is the vector $\mathbf{e}_k$. Similarly, $\mathbf{Q}$ denotes the $n\times p$ matrix, whose kth column is the vector $\tilde{\mathbf{e}}_k$. The first approach to obtain the biorthogonality relation between the bases is to find $\mathbf{Q}$ such that $\mathbf{PQ}^*=\mathbf{1}_n$, where $\mathbf{1}_n$ is the $n\times n$ identity matrix, but the matrix $\mathbf{P}$ is poorly conditioned and its numerical inverse can include significant roundoff errors. Another approach is to directly use the definition of $\tilde{\mathbf{e}}_k$; indeed, from $\zeta_i\Psi_i=K_n^*\tilde{\mathbf{e}}_i$, we deduce that: $\zeta_i\mathbf{e}_i=(K_nK_n^*)\tilde{\mathbf{e}}_i$. The *Gram matrix* $\mathbf{M}_n$ of the operator $K_nK_n^*$ is usually well conditioned, it is symmetric and can be inverted. We can then define $\tilde{\mathbf{e}}_k=\mathbf{M}_n^{-1}\mathbf{e}_k$; note that here, by construction, we have $\zeta_k=1$.

Returning to our rheometry problem, we find that an estimate of the shear rate is obtained by computing from a set of n data $\mathbf{w}=\omega_1,\omega_2,\ldots,\omega_n$:

$$\tilde{\dot{\gamma}}(\tau)=\sum_{i=1}^{n}[\mathbf{w},\tilde{\mathbf{e}}_i]\Psi_i(\tau). \tag{A1}$$

B. Numerical implementation

The numerical implementation requires (i) the selection of a representation for $\dot{\gamma}$ (see the EPAPS document) and the definition of the basis Ψ_i, (ii) the computation of the images $\mathbf{e}_i=K_n\Psi_i$ and the resulting $n\times p$ matrix $\mathbf{P}$, (iii) the computation of the $n\times n$ Gram matrix $\mathbf{M}_n$, (iv) computation of the dual vectors $\tilde{\mathbf{e}}_i$, and (v) computation of the shear rate [Eq. (A1)]. Note that steps (i)–(iv) are independent of measurements and can be done once (for a given radius ratio β). The matrix $\mathbf{P}$ must be calculated numerically. The Gram matrix $\mathbf{M}_n$ can be computed analytically since its entries are given by

$$M_{ij}=\int_{\mathbb{R}}\frac{dx}{x}H[(x-\beta\tau_i)(\tau_i-x)]H[(x-\beta\tau_j)(\tau_j-x)]=\ln\left(\frac{x_2}{x_1}\right),$$

where $[x_1,x_2]=[\beta\tau_i,\tau_i]\cap[\beta\tau_j,\tau_j]$. The Gram matrix is usually well-conditioned even though many entries are zero. It can be inverted easily by the usual methods.

C. Numerical example

We consider the same example as in Sec. III D. We consider $n=100$ data computed from Eq. (10), $\mathbf{w}:\omega_i=\Omega(T_i)$, where $T_i=i\delta$ for $0\leqslant i\leqslant n-1$ and $\delta=(n-1)^{-1}$. The shear rate is sought in terms of a multiresolution wavelet series (see the EPAPS document). As previously in Sec. III D, we use the Daubechies D8 wavelets and we take $\beta=0.5$. Figure 5 shows the recovered dimensionless shear rate when D8 wavelets are used with $p=16$ (a), $p=32$ (b), and $p=128$ (c).

As seen in Fig. 5(a), there is a satisfactory agreement between the recovered and exact shear rates for a fairly small number of wavelets ($p=16$), but this agreement is poor at the boundaries; this problem results from the use of periodized wavelets (see the EPAPS document). Interestingly, increasing the wavelet number p reduces the problems encountered at the boundaries, but also causes new problems: for $T\approx 0.5$, a small bump deforms the retrieved flow curve for $p=32$ [see Fig. 5(b)]. Still, increasing the number of wavelets aggravates this problem, as shown on panel (c) of Fig. 5: the bump is replaced by a series of wide oscillations. Typically, increasing p here leads to the mean-square error rising (7.23×10^{-5} from 1.25×10^{-4} to 1.25×10^{-4} when p is increased from 32 to 128). There is also a typical distance separating the oscillations, which is controlled by the radius ratio β. For instance, on panel (c), the first oscillations are localized around $T\approx 0.5$, the second close to $\beta\times 0.5=0.25$, the third to $\beta^2\times 0.5=0.125$, and so on in a geometrical progression.

The reason for these shortcomings stems from the fact that, from the analytical viewpoint, the dual function u_i involves an infinite series of increasing terms, but its discrete counterpart $\tilde{\mathbf{e}}_i$ is unable to mimic the behavior of higher terms in this series. To illustrate this more clearly, let us consider an example by examining what happens for high-order vaguelettes. In Fig. 6, we have plotted the dual function $u_{4,8}$ (dashed line) associated with the wavelet $\Psi_{25}=\psi_{4,8}$ and its discrete counterpart $\tilde{\mathbf{e}}_{25}$; only the first four terms in the infinite series $u_{4,8}$ [see Eq. (6)] have been reported for the plot to be readable. For x in the range 0.2–1, there is reasonably good agreement between the discrete values $\tilde{\mathbf{e}}_{25}$ and the

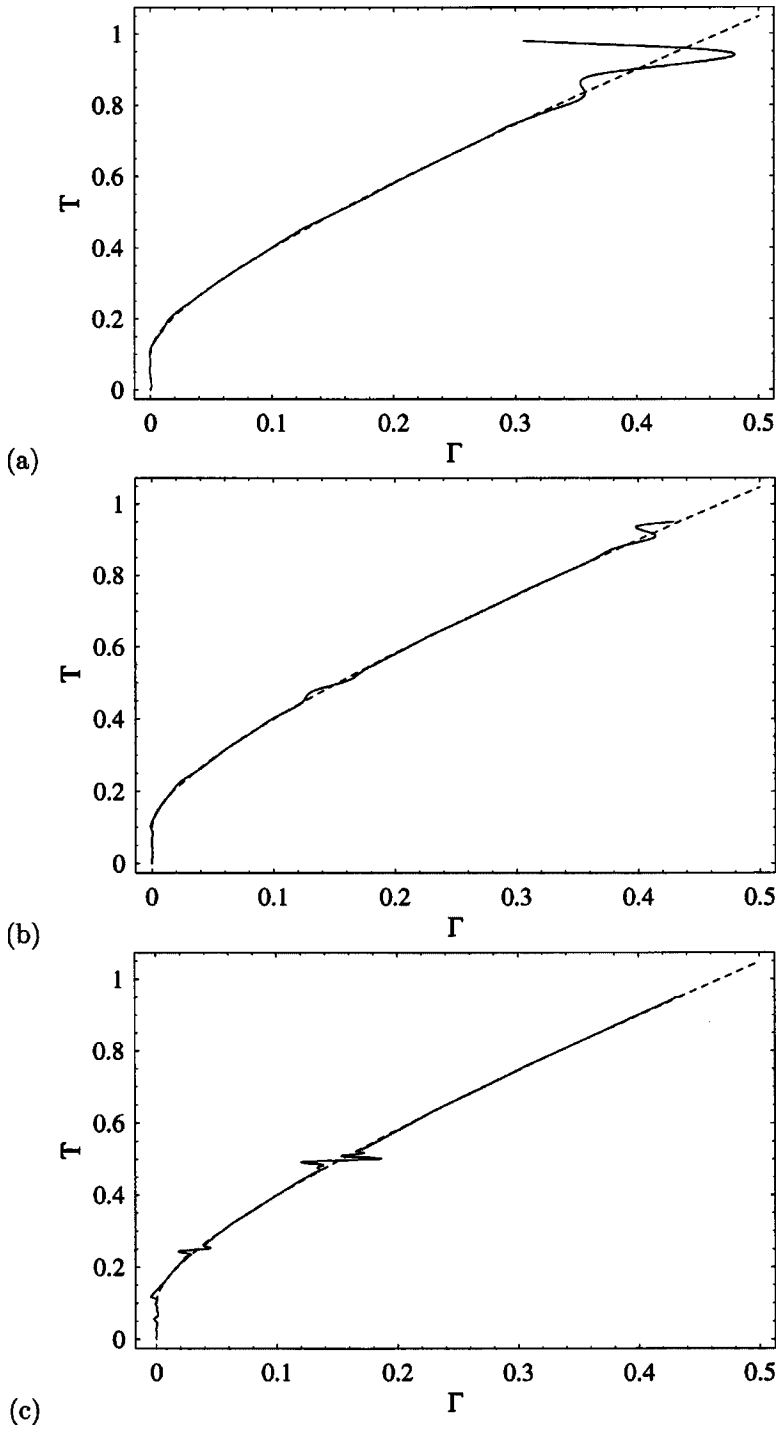

FIG. 5. (a) Flow curve for the (dimensionless) Casson model when $p=2^4=16$ wavelets are used to represent $\dot{\gamma}$; the solid line represents the numerical approximation obtained by using the discrete WVD approach, whereas the dashed line represents the exact solution [Eq. (9)]. (b) Flow curve when $p=2^5=32$ wavelets are used. (c) Flow curve when $p=2^7=128$ wavelets are used.

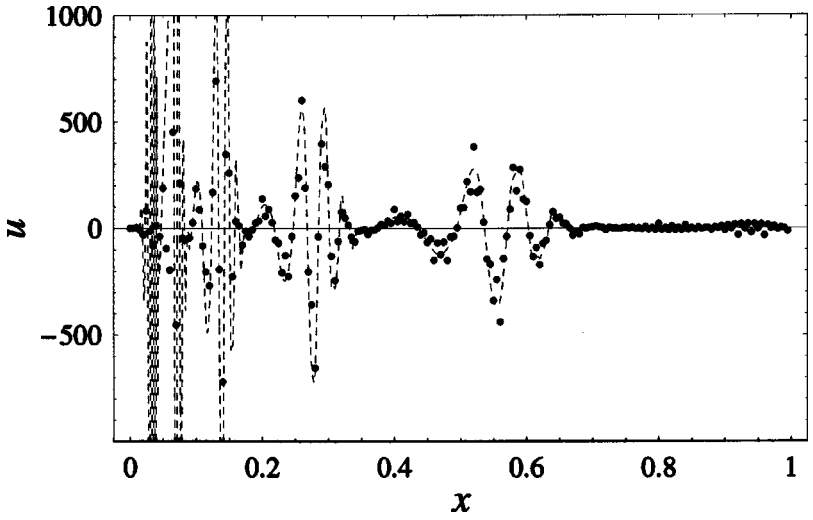

FIG. 6. Comparison between the dual function $u_{4,8}$ (dashed line, truncated series) and its discrete counterpart $\tilde{\mathbf{e}}_{25}$.

dual function $u_{4,8}$: points fall onto the first two oscillations corresponding to $U_0'(x)$ and $\beta^{-1}U'(\beta^{-1}x)$ in the infinite series [see Eq. (6)]. The third oscillation corresponds to $\beta^{-2}U'(\beta^{-2}x)$; its support is much narrower and its amplitude larger than the two previous oscillations; the points do not capture all the oscillations. The only way for the vector $\tilde{\mathbf{e}}_{25}$ to mimic high-order terms of u_{25} would be to substantially increase the point density, i.e., the measurement number n.

In short, the discrete WVD decomposition can provide results in fairly good agreement with data (except for the boundaries where spurious oscillations are induced because of the use of periodized wavelets). Increasing the accuracy of the reconstructed shear-rate requires substantially raising the measurement number for the discrete vaguelette to mimic the continuous-vaguelette behavior. Its advantage is less obvious compared to Tikhonov regularization and the continuous formulation of the WVD decomposition even though, with modern rheometers, taking a large number of measurements is rather easy.

References

Abramovich, F., and B. Silverman, "Wavelet decomposition approaches to statistical inverse problems," Biometrika **85**, 115–129 (1998).

Ancey, C., "Role of lubricated contacts in concentrated polydisperse suspensions," J. Rheol. **45**, 1421–1439 (2001).

Baudez, J., S. Rodts, X. Chateau, and P. Coussot, "New technique for reconstructing instantaneous profiles from viscometric tests: Application to pasty materials," J. Rheol. **48**, 69–82 (2004).

Bertero, M., C. De Mol, and E. Pike, "Linear inverse problems with discrete data. I: General formulation and singular system analysis," Inverse Probl. **1**, 301–330 (1985).

Bertero, M., C. De Mol, and E. Pike, "Linear inverse problems with discrete data. II: Stability and regularization," Inverse Probl. **4**, 573–594 (1988).

Borgia, A., and F. Spera, "Error analysis for reducing noisy wide-gap concentric cylinder rheometric data for nonlinear fluids: Theory and applications," J. Rheol. **34**, 117–135 (1990).

Cai, T., "Adaptative wavelet estimation: A block thresholding and oracle inequality approach," Ann. Stat. **27**, 898–924 (1999).

Cai, T., "On adaptive wavelet estimation of a derivative and other related linear inverse problems," J. Stat. Plan. Infer. **108**, 329–349 (2002).

Champier, S., and L. Grammont, "A wavelet-vaguelet method for unfolding sphere size distributions," Inverse Probl. **18**, 79–94 (2002).

Coleman, B., H. Markowitz, and W. Noll, *Viscometric Flows of Non-Newtonian Fluids, Springer Tracts in Natural Philosophy* Vol. 5 (Springer, Berlin, 1966).

Coussot, P., "Structural similarity and transition from Newtonian to non-Newtonian behavior for clay-water suspensions," Phys. Rev. Lett. **20**, 3971–3974 (1995).

Darby, R., "Couette viscometer data reduction for materials with a yield stress," J. Rheol. **29**, 369–378 (1985).

Dicken, V., and P. Maass, "Wavelet-Galerkin methods for ill-posed problems," J. Inv. Ill-Posed Problems **4**, 203–221 (1996).

Donoho, D., "Nonlinear solution of linear inverse problems by wavelet-vaguelette decomposition," Appl. Comput. Harmon. Anal. **2**, 101–126 (1995).

Donoho, D., and I. Johnstone, "Wavelet shrinkage: Asymptotia?," J. R. Stat. Soc. Ser. B. Methodol. **57**, 301–369 (1995).

Friedrich, C., J. Honerkamp, and J. Weese, "New ill-posed problems in rheology," Rheol. Acta **35**, 186–193 (1996).

Gamboa, F., and E. Gassiat, "Bayesian methods and maximum entropy for ill-posed inverse problems," Ann. Stat. **25**, 328–350 (1997).

Golberg, M., "A method of adjoints for solving some ill-posed equations of the first kind," Appl. Math. Comput. **5**, 123–130 (1979).

Hart, J., *Nonparametric Smoothing and Lack-of-Fit Tests* (Springer, New York, 1999).

Kolaczyk, E., "A wavelet shrinkage approach to tomographic image reconstruction," J. Am. Stat. Assoc. **91**, 1079–1090 (1996).

Kovac, A., "Wavelet thresholding for unequally spaced data," Ph.D. thesis, University of Bristol, 1998.

Krieger, I., and H. Elrod, "Direct determination of the flow curves of non-Newtonian fluids. II Shearing rate in the concentric cylinder viscometer," J. Appl. Phys. **24**, 134–136 (1953).

Krieger, I., and S. Maron, "Direct determination of the flow curves of non-Newtonian fluids," J. Appl. Phys. **23**, 147–149 (1952).

Leong, Y., and Y. Yeow, "Obtaining the shear stress shear rate relationship and yield of liquid foods from Couette viscometry data," Rheol. Acta **42**, 365–371 (2003).

Lootens, D., H. Van Damme, and P. Hébraud, "Giant stress fluctuations at the jamming transition," Phys. Rev. Lett. **90**, 178301 (2003).

Louis, A., "A unified approach to regularization methods for linear and ill-posed problems," Inverse Probl. **15**, 489–498 (1999).

Louis, A., P. Maass, and A. Rieder, *Wavelets, Theory and Applications*, Pure & Applied Mathematics (Wiley, Chichester, 1997).

Macsporran, W., "Direct numerical evaluation of shear rates in concentric cylinder viscometry using least-squares cubic splines," J. Rheol. **33**, 745–755 (1989).

Mooney, M., "Explicit formulas for slip and fluidity," J. Rheol. **2**, 210–222 (1931).

Mosegaard, K., and M. Sambridge, "Monte Carlo analysis of inverse problems," Inverse Probl. **18**, R29–R54 (2002).

Nguyen, Q., and D. Boger, "Measuring the flow properties of yield stress fluids," Annu. Rev. Fluid Mech. **24**, 47–88 (1992).

O'Sullivan, F., "A statistical perpective on ill-posed inverse problems," Stat. Sci. **1**, 502–527 (1986).

Raynaud, J., P. Moucheront, J. Baudez, F. Bertrand, J. Guilbaud, and P. Coussot, "Direct determination by nuclear magnetic resonance of the thixotropic and yielding behavior of suspensions," J. Rheol. **46**, 709–732 (2002).

Rieder, A., "A wavelet multilevel method for ill-posed problems stabilized by Tikhonov regularization," Numer. Math. **75**, 501–522 (1997).

Roberts, G., and H. Barnes, "New measurements of the flow-curves for Carbopol dispersions without slip artifacts," Rheol. Acta **40**, 499–503 (2001).

Tanner, R., and G. Williams, "Iterative numerical methods for some integral equations arising in rheology," Trans. Soc. Rheol. **14**, 19–38 (1970).

Tenorio, L., "Statistical regularization of inverse problems," SIAM Rev. **43**, 347–366 (2001).

Wahba, G., *Spline Models for Observational Data* (Society for Industrial and Applied Mathematics, Philadelphia, 1990).

Werman, M., and D. Keren, "A Bayesian method for fitting parametric and nonparametric models to noisy data," IEEE Trans. Pattern Anal. Mach. Intell. **23**, 528–534 (2001).

Yang, T., and I. Krieger, "Comparison of methods for calculating shear rates in coaxial viscometers," J. Rheol. **22**, 413–421 (1978).

Yeow, Y., W. Ko, and P. Tang, "Solving the inverse problem of Couette viscometry by Tikhonov regularization," J. Rheol. **44**, 1335–1351 (2000).

See **EPAPS** Document No. E-JORHD2-49-003502 for the mathematical proofs and a Mathematica program for numerical applications. This document may be retrieved via the EPAPS homepage (http://www.aip.org/pubservs/epaps.html) or from ftp.aip.org in the directory/epas/. See the EPAPS homepage for more information.